PHOTONICS Research

Spatial cage solitons—taming light bullets

Chao Mei,[1,2] Ihar Babushkin,[3] Tamas Nagy,[1] and Günter Steinmeyer[1,4,*]

[1]Max Born Institute for Nonlinear Optics and Short Pulse Spectroscopy, 12489 Berlin, Germany
[2]School of Computer and Communication Engineering, University of Science and Technology Beijing (USTB), Beijing 100083, China
[3]Institute of Quantum Optics, Leibniz University Hannover, 30167 Hannover, Germany
[4]Institut für Physik, Humboldt Universität zu Berlin, 12489 Berlin, Germany
*Corresponding author: steinmey@mbi-berlin.de

Received 26 July 2021; revised 20 October 2021; accepted 25 October 2021; posted 2 November 2021 (Doc. ID 438610); published 16 December 2021

Multimode nonlinear optics is used to overcome a long-standing limitation of fiber optics, tightly phase locking several spatial modes and enabling the coherent transport of a wave packet through a multimode fiber. A similar problem is encountered in the temporal compression of multimillijoule pulses to few-cycle duration in hollow gas-filled fibers. Scaling the fiber length to up to 6 m, hollow fibers have recently reached 1 TW of peak power. Despite the remarkable utility of the hollow fiber compressor and its widespread application, however, no analytical model exists to enable insight into the scaling behavior of maximum compressibility and peak power. Here we extend a recently introduced formalism for describing mode locking to the analog scenario of locking spatial fiber modes together. Our formalism unveils the coexistence of two soliton branches for anomalous modal dispersion and indicates the formation of stable spatiotemporal light bullets that would be unstable in free space, similar to the temporal cage solitons in mode-locking theory. Our model enables deeper understanding of the physical processes behind the formation of such light bullets and predicts the existence of multimode solitons in a much wider range of fiber types than previously considered possible.

https://doi.org/10.1364/PRJ.438610

1. INTRODUCTION

Spatial solitons have fascinated researchers since the early days of nonlinear optics [1,2]. In combination with self-phase modulation, the self-focusing effect offers the possibility for three-dimensional contraction of an optical wave packet and a concomitant intensity increase. While there exist numerous reports on such light bullets [3–5], this intriguing nonlinear mechanism found little application, probably because of the limiting action of a spatial modulation instability [6,7]. Starting from small imperfection in the beam profile, this process induces a rapid small-scale breakup of the beam profile into filaments when the critical power P_{crit} is exceeded [8,9], thus limiting the obtainable nonlinear interaction length. Given this severe constraint, high-power pulse compression and nonlinear conversion techniques have resorted to hollow capillaries for extended nonlinear interaction length [10–13]. While several other competing techniques [14,15] have been discussed for the compression of pulses with gigawatt peak powers, the hollow fiber is currently the most established compression technique and has found widespread application in attosecond pulse generation and other high-field experiments; see, e.g., Refs. [16,17]. Utilizing the advanced stretched-fiber technique [18,19] recently enabled record-breaking continuous powers above 300 W [20] and peak powers exceeding 1 TW for the first time [21]. Despite the widespread utility of this technique, however, there exist only relatively few analytical approaches [22,23] for modeling the nonlinear broadening processes inside the hollow fiber. Numerical simulations often resorted to a simplified one-dimensional approximation, as full modal expansions [24–26] are numerically cumbersome. In the following, we present a completely analytical approach for determining spatial soliton solutions in nonlinear multimode fiber geometries. Similar spatiotemporal solitons have previously been observed in numerical simulations [27,28]. Moreover, our approach is mathematically similar to the cage soliton solutions of the Haus master equation of mode locking [29,30], and it is also applicable for the thriving field of multimode fiber nonlinear optics [31–36]. Assuming adiabatic pulse shaping, the results of this analysis enable the derivation of universal scaling laws for the design of nonlinear multimode waveguides.

2. THE MARCATILI-SCHMELTZER MODEL

The linear optical properties of a cylindrical hollow dielectric waveguide with radius a were first modeled by Marcatili and Schmeltzer [10]. Assuming linear polarization, one finds hybrid solutions of the wave equation, which were originally designated as EH_{mn} modes. In solid core multimode (SCM) fibers,

widely similar solutions are referred to as $LP_{(m-1)n}$ modes. Strictly speaking, both designations are not identical because of the Goos–Hänchen effect [37], which causes the $LP_{(m-1)n}$ modes to extend into the cladding. In contrast, the EH_{mn} modes exhibit a node of the electric field at the dielectric interface. Assuming $m = 1$, i.e., azimuthal homogeneity, the radial field profile of the EH_{1n} mode is given by

$$E_n(r) \propto J_0\left(\frac{u_n r}{a}\right), \tag{1}$$

with the zero-order Bessel function J_0 and its nth zero u_n ($n > 0$); see Fig. 1(a). The complex-valued propagation constant of these modes is given by

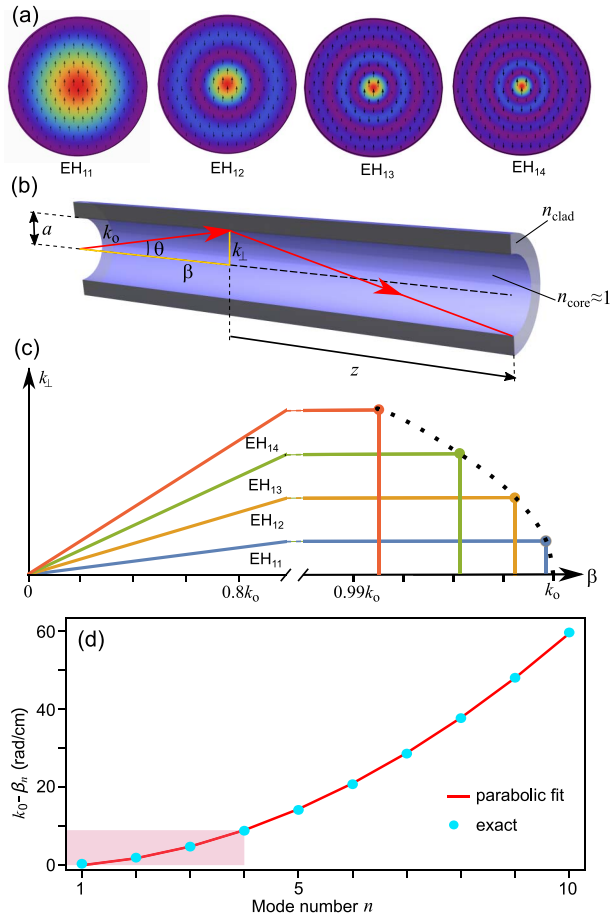

Fig. 1. (a) Mode fields of the first four EH_{1n} modes considered in this study. Intensities are depicted by colors, and electric fields are represented by arrows. (b) Ray-optical representation of hollow-fiber transmission. The wave vector k_0 can be decomposed into a transverse component $k_\perp$ and a longitudinal component β, which are connected by Pythagoras' theorem [38]. (c) The propagation constants β_n of the individual EH_{1n} modes follow an approximate n^2 dependence, whereas the $k_{\perp,n}$ underly a linear relationship with n. (d) Intramode dispersion, deviation of the propagation constants of the first 10 EH_{1n} modes from the propagation constant of a plane wave, calculated at 800 nm wavelength for an HCF with a core radius of 100 μm; symbols, exact solution according to Eq. (3); curve, parabolic fit; the four modes of interest within this study are highlighted in red, indicating a dephasing of ≈8 rad/cm in the linear optical regime.

$$\kappa_n = \beta_n + i\alpha_n = k_0 - \frac{u_n^2}{2k_0 a^2}\left(1 - i\frac{\epsilon + 1}{k_0 a\sqrt{\epsilon - 1}}\right), \tag{2}$$

where $k_0 = 2\pi/\lambda$ is the wavenumber and $\sqrt{\epsilon} = n_{\text{clad}}$ the refractive index of the cladding material. Here β_n denotes the propagation constant of the nth mode. The propagation constant varies with the eigenmode, which causes intermodal dispersion and is attributed to diffractive effects. α_n describes mode-dependent losses in a hollow-fiber geometry. Exploiting the trigonometric relationship between the propagation constant and the wavenumber displayed in Figs. 1(b) and 1(c), one finds an approximate parabolic dependence [38,39] of the propagation constant,

$$\beta_n = k_0 \cos\left(\frac{u_n}{k_0 a}\right) \approx \beta_1 - \frac{\pi^2 (n-1)^2}{2k_0 a^2} = \beta_1 + \mathcal{B}(n-1)^2. \tag{3}$$

Here β_1 is the propagation constant of the fundamental mode, and $\mathcal{B}$ describes intermodal dispersion due to diffraction. A negative value of $\mathcal{B}$ is formally equivalent to anomalous group-velocity dispersion in the formation of time-domain solitons. The quality of the approximation is depicted in Fig. 1(d), clearly indicating the close analogy between diffraction and dispersion for the formation of spatial and temporal solitons, respectively. In order to show that small deviations from a perfect parabolic dependence in Eq. (3) play no major role, we used the exact relationship in computing all of the following example cases. The identical parabolic approximation can be made for SCM fibers [40], yet with positive curvature $\mathcal{B}$. Exploiting the general relation,

$$\beta^2 + k_\perp^2 = k_0^2 \sin^2\theta + k_0^2 \cos^2\theta = k_0^2, \tag{4}$$

depicted in Fig. 1(c) and reinserting discretized values β_n and $\theta_n = u_n/k_0 a$, one also finds an approximate linear relationship for the transverse wavenumber,

$$k_{\perp,n} = k_0 \sin\left(\frac{u_n}{k_0 a}\right) \approx \left(n - \frac{1}{4}\right)\frac{\pi}{a}. \tag{5}$$

3. EXPANSION TO NONLINEAR WAVEGUIDES

In the following, we describe the evolution of the spatial beam profile $E(z, r)$ upon propagation along the coordinate z with the transverse wave equation,

$$\partial_z E = \frac{i\beta}{r}\partial_r r \partial_r E + i\Gamma|E|^2 E. \tag{6}$$

The first term on the right-hand side describes linear diffractive effects, where $\beta = k_0 = 2\pi/\lambda$ is typically assumed for a plane wave propagating in vacuum. In contrast, as $\beta_n < k_0$ in a hollow waveguide, the modes E_n propagate at superluminal phase velocity inside, which can be explained by $-\pi$ phase jumps due to Fresnel reflection at the interface in the geometrical optical picture of Refs. [38,39]. The second term on the right-hand side of Eq. (6) is not included in the linear optical description of Marcatili and Schmeltzer [10] and describes self-focusing effects scaling with $\Gamma = k_0 n_2$, where the nonlinear refractive index is given by n_2. These self-focusing effects are the source of mode mixing, i.e., energy flow between the eigenmodes (mostly towards higher-order modes) and lead to the shrinkage of the

beam analogously to free-space propagation. Equation (6) is widely similar to the nonlinear Schrödinger equation (NLSE), yet with the temporal coordinate t replaced by the radial coordinate r. While it is customary to numerically solve the NLSE by a split-step Fourier method [41], the equation can be reformulated in the spatial frequency domain [30], which is also known as $k_\perp$ space and leads to a system of nonlinearly coupled ordinary differential equations. Consequently, rewriting Eq. (6) in the $k_\perp$ domain leads to a similar system of coupled equations [27,42],

$$\partial_z \tilde{E}_n = i\beta_n \tilde{E}_n + i\Gamma \sum_{j+k-\ell=n} \tilde{E}_j \tilde{E}_k \tilde{E}_\ell^*. \tag{7}$$

Here the product $|E|^2E$ is now replaced by a double-correlation sum, which is essentially exploiting the Wiener–Khinchin autocorrelation theorem [43]. The correlation sum can also be understood as conservation of the transverse wavenumber $k_\perp$ in Fig. 1(b), leading to the constraint $n = j + k - \ell$. The partially degenerate case $j = k$ is also known as self-diffraction [44]. As was noted by DeLong *et al.* [45], the self-diffraction process is not exactly phase-matched. This slight mismatch is accounted for by the intermodal dispersion term $\beta_n \tilde{E}_n$, which takes the part of group-delay dispersion with its quadratic dependence in the frequency representation of the Haus master equation [30]. As the parabolic dependence on mode number n is convex for hollow fibers, one can associate this case with anomalous dispersion, whereas SCM fibers display normal modal dispersion. Moreover, the slight phase mismatch can be understood with the neglect of the linear term in Eq. (3) and is otherwise similar to higher-order dispersion contributions in traditional mode-locking theory [29], i.e., these contributions give rise to deviations from equidistance of the cold cavity modes. Solving the mode-locking version of Eq. (7) requires restrictive assumptions on the number of coupled longitudinal modes [30]. In the transverse case, it is often considered sufficient to include only a few spatial modes (e.g., $N = 3$ [26]) for treating nonlinear propagation through a hollow waveguide. We therefore write out Eq. (7) for four modes, which effectively converts the problem of finding an eigensolution of a set of ordinary differential equations into the problem of finding a root of a system of nonlinearly coupled algebraic equations. In the following, we use excessive content in $\tilde{E}_4$ as an indicator for the breakdown of our simplifying assumptions,

$$\begin{aligned}
\partial_z \tilde{E}_1 &= i\beta_1 \tilde{E}_1 + i\Gamma[\eta_{1234} \tilde{E}_2 \tilde{E}_3 \tilde{E}_4^* + \eta_{123} \tilde{E}_2^2 \tilde{E}_3^* \\
&\quad + (|\tilde{E}_1|^2 + \eta_{12}|\tilde{E}_2|^2 + \eta_{13}|\tilde{E}_3|^2 + \eta_{14}|\tilde{E}_4|^2)\tilde{E}_1], \\
\partial_z \tilde{E}_2 &= i\beta_2 \tilde{E}_2 + i\Gamma[\eta_{1234} \tilde{E}_1 \tilde{E}_3^* \tilde{E}_4 + \eta_{123} \tilde{E}_1 \tilde{E}_2^* \tilde{E}_3 + \eta_{234} \tilde{E}_3^2 \tilde{E}_4^* \\
&\quad + (\eta_{12}|\tilde{E}_1|^2 + |\tilde{E}_2|^2 + \eta_{23}|\tilde{E}_3|^2 + \eta_{24}|\tilde{E}_4|^2)\tilde{E}_2], \\
\partial_z \tilde{E}_3 &= i\beta_3 \tilde{E}_3 + i\Gamma[\eta_{1234} \tilde{E}_1 \tilde{E}_2^* \tilde{E}_4 + \eta_{123} \tilde{E}_1^* \tilde{E}_2^2 + \eta_{234} \tilde{E}_2 \tilde{E}_3^* \tilde{E}_4 \\
&\quad + (\eta_{13}|\tilde{E}_1|^2 + \eta_{23}|\tilde{E}_2|^2 + |\tilde{E}_3|^2 + \eta_{34}|\tilde{E}_4|^2)\tilde{E}_3], \\
\partial_z \tilde{E}_4 &= i\beta_4 \tilde{E}_4 + i\Gamma[\eta_{1234} \tilde{E}_1^* \tilde{E}_2 \tilde{E}_3 + \eta_{234} \tilde{E}_2^* \tilde{E}_3^2 (\eta_{14}|\tilde{E}_1|^2 \\
&\quad + \eta_{24}|\tilde{E}_2|^2 + \eta_{34}|\tilde{E}_3|^2 + |\tilde{E}_4|^2)\tilde{E}_4].
\end{aligned} \tag{8}$$

Here the β_n terms describe intermodal dispersion, i.e., the phase velocity differences between the individual modes. Self-diffraction is accounted for by partially degenerate four-wave mixing (FWM) terms $\propto \eta_{k\ell} \tilde{E}_k^2 E_\ell^*$. Self-focusing of the individual modes is described by the fully degenerate terms $\propto |E_k|^2 E_k$. In addition, cross-phase modulation (XPM) terms appear; cf. Table 1. In Eq. (8), we introduced modal overlap factors η_{nj}, η_{njk}, and $\eta_{njk\ell}$ for noncollinear FWM processes as they have been previously discussed in Refs. [42,46]. For the fully nondegenerate process, we define

$$\eta_{njk\ell} = \frac{\int_0^a \tilde{E}_n \tilde{E}_j \tilde{E}_k \tilde{E}_\ell r \mathrm{d}r}{\prod_{m=\{n,j,k,\ell\}} \sqrt[4]{\int_0^a \tilde{E}_m^4 r \mathrm{d}r}}. \tag{9}$$

For degenerate mixing processes, we use a shorthand notation, e.g., $\eta_{1221} = \eta_{2112} = \eta_{12}/2$ and include the degeneracy factor in the respective overlap factors. Values for the various η are listed in Table 1. Provided that the nonlinear length L_{NL} is much shorter than the dispersive length L_D [41], Eq. (8) can be used as a highly efficient tool for simulating the propagation via solving a set of coupled ordinary differential equations. As will be further discussed below, such adiabaticity can be assumed in typical hollow-fiber compression scenarios. Moreover, propagation losses can be accounted for by a complex-valued redefinition of the β_n.

4. SOLITON SOLUTIONS

Assuming propagation of the $\tilde{E}_j$ at identical phase velocity, i.e., as a solitonic wave packet, we find a wavenumber offset ψ relative to the fundamental mode β_1. We further renormalize real-valued electric field amplitudes $a_n = |\tilde{E}_n/\tilde{E}_1|$ to yield $a_1 = 1$ and redefine an effective nonlinearity $\gamma = \Gamma \mathcal{B}^{-1} |\tilde{E}_1|^{-2}$. Using these simplifications, we can extract an algebraic discriminant for the resulting spatial soliton,

$$\begin{aligned}
\psi &= \gamma(1 + \eta_{1234} a_2 a_3 a_4 + \eta_{123} a_2^2 a_3 + \eta_{12} a_2^2 + \eta_{13} a_3^2 + \eta_{14} a_4^2) \\
&= \gamma[\eta_{1234} a_3 a_4 + \eta_{123} a_2 a_3 + \eta_{234} a_3^2 a_4 \\
&\quad + (\eta_{12} + a_2^2 + \eta_{23} a_3^2 + \eta_{24} a_4^2) a_2] + a_2 \\
&= \gamma[\eta_{1234} a_2 a_4 + \eta_{123} a_2^2 + \eta_{234} a_2 a_3 a_4 \\
&\quad + (\eta_{13} + \eta_{23} a_2^2 + a_3^2 + \eta_{34} a_4^2) a_3] + 4a_3 \\
&= \gamma[\eta_{1234} a_2 a_3 + \eta_{234} a_2 a_3^2 \\
&\quad + (\eta_{14} + \eta_{24} a_2^2 + \eta_{34} a_3^2 + a_4^2) a_4] + 9a_4.
\end{aligned} \tag{10}$$

One can now retrieve all real-valued roots of Eq. (10) and compute beam diameter w_{eff}, loss α_{eff}, and, most importantly, the resulting "soliton phase" ψ [47], which is more correctly defined as the total propagation constant involving both linear and nonlinear effects relative to the phase velocity frame. ψ vanishes for $\gamma \to 0$, as we already accounted for linear propagation effects by subtracting the propagation constant β_1 in Eq. (10).

Table 1. Nonlinear Mode-Coupling Factors[a]

XPM	$\eta_{12} = 1.709$	$\eta_{13} = 1.529$	$\eta_{14} = 1.408$
XPM	$\eta_{23} = 1.847$	$\eta_{24} = 1.725$	$\eta_{34} = 1.897$
FWM	$\eta_{123} = 0.788$	$\eta_{234} = 0.874$	$\eta_{1234} = 1.462$

[a]Nondegenerate FWM, $\eta_{njk\ell}$; degenerate FWM, $\eta_{njk} = \eta_{nnjk}$; XPM, $\eta_{nj} = \eta_{njjn}$.

This effective subtraction of the linear propagation phase now gives immediate access to the nonlinear phase via $\partial\varphi_{\mathrm{nl}}/\partial z = \psi$. Using the relation $\varphi_{\mathrm{nl}} = k_0 z n_2 P A_{\mathrm{eff}}^{-1}$ with the nonlinear refractive index n_2 and the effective area [41] of the fundamental EH_{11} mode,

$$A_{\mathrm{eff}} = \frac{1}{2\pi}\frac{\left(\int |E(r)|^2 r\mathrm{d}r\right)^2}{\int |E(r)|^4 r\mathrm{d}r} \approx 1.50a^2, \tag{11}$$

one can then relate the soliton phase to the power P in the nonlinear waveguide. Inserting the definition of the critical power for self-focusing $P_{\mathrm{cr}} = 0.147\lambda^2/n_2$ [8,9,23], we then finally yield

$$P \approx 10.2 P_{\mathrm{cr}} \frac{\psi a^2}{k_0 \lambda^2}. \tag{12}$$

The resulting peak power versus effective nonlinearity is depicted in Fig. 2(a). In the anomalous regime (hollow fibers), the higher-order modes EH_{1n}, $n > 1$ of the spatial soliton solutions carry the opposite sign of the fundamental EH_{11} mode. This can be understood by a partial cancellation of nonlinearity and modal dispersion, similar to the formation of Schrödinger solitons [2]. In turn, a depression of the peak intensity and an increased effective area A_{eff} of the beam profile result [Fig. 2(b)]. Consequently, the hollow waveguide can host beams with a peak power of $\approx 1.4P_{\mathrm{cr}}$, yet at a characteristic donut profile; cf. Fig. 3. In the normal dispersion regime (SCM fibers), peak intensities are enhanced as nonlinearity and modal dispersion add up, leading to cusp-like beam profiles for $\kappa > 0$. Comparing both waveguide dispersion regimes, it is striking that the asymmetry in the $P(\gamma)$ relation is only caused by beam profile variations. For the SCM case, this effect leads to a maximum peak power hosting of $0.5P_{\mathrm{cr}}$. Apart from these two fundamental soliton branches, our investigation identifies a second solution branch in the anomalous dispersion regime (red curves in Fig. 2). In this branch, the limit-value donut solution converges toward a "Mexican hat" solution upon subsequent reduction of power. Because of this positive feedback on the losses, the increasing amount of energy in the lossy higher-order modes leads to a runaway, i.e., this solution branch is unstable. This situation can therefore be understood as a blowup of the beam profile in $k_\perp$ space, i.e., the energy is quickly transferred into increasingly lossy higher-order modes. In contrast, the fundamental soliton branches (blue and green in Fig. 2) self-stabilize upon propagation as their higher-order contents reduce with decreasing peak power, i.e., there is a negative feedback mechanism.

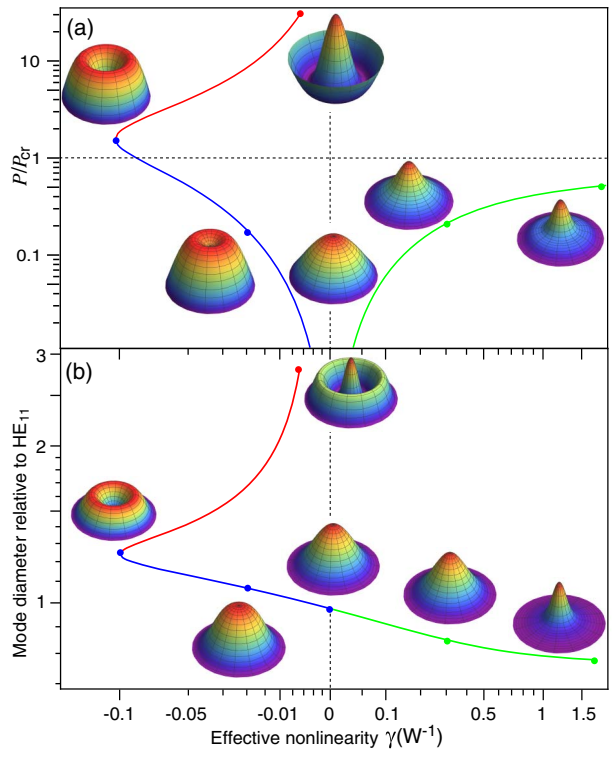

Fig. 2. Spatial soliton solution branches of Eq. (8). For normal modal dispersion ($n_{\mathrm{core}} > n_{\mathrm{clad}}$), a single solution branch exists (green). In hollow fibers, two branches coexist (blue and red). The red branch is considered unstable (see discussion in text). (a) Radially integrated intensity $\int E(r)^2 r\mathrm{d}r = P$ of the spatial cage soliton solutions versus effective nonlinearity. Powers have been normalized to the critical power of self-focusing P_{cr} in free space [9]. Insets show $E(r)$ for parameters indicated by symbols. (b) Root mean square mode diameter of spatial solitons normalized to the HE_{11} mode; insets show spatial intensity profiles $|E(r)|^2$.

To this end, it appears illustrative to compute the relevant interaction lengths [41] inside a hollow fiber. Given the rather low group-velocity dispersion of noble gases like argon, which may be additionally cancelled out by the waveguide (group-velocity) dispersion of the hollow fiber, dispersion lengths $L_D \approx \tau^2/|\beta_2|$ for pulse durations $\tau_0 > 20$ fs generally exceed the fiber length by a large factor for experimental conditions for typical hollow-fiber compressors in Refs. [19–21]. The absorption length is commonly also chosen longer than the actual fiber length. This is contrasted by the nonlinear length $L_{\mathrm{NL}} = \Gamma^{-1}P^{-1}$, which amounts to only a few millimeters for powers $P > 0.1P_{\mathrm{cr}}$ at identical experimental conditions. One can therefore conclude that spatial soliton effects strongly dominate the nonlinear dynamics inside the hollow fiber, causing an adiabatic reshaping of the solitons as a reaction

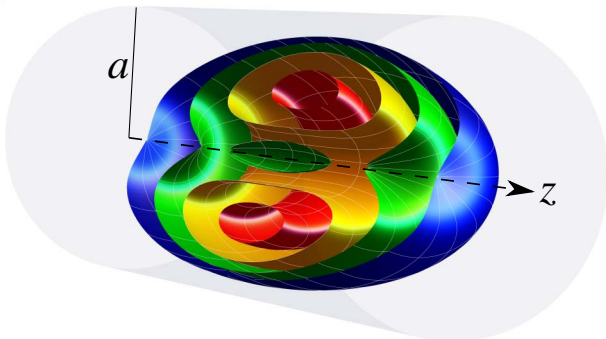

Fig. 3. Three-dimensional visualization of the light bullet structure at the stability limit ($\approx 1.4P_{\mathrm{cr}}$) in the anomalous modal dispersion regime. Equi-intensity surfaces are shown with colors red (80% peak intensity) to blue (10% peak intensity). In the center, a donut structure dominates, which evolves into an ellipsoidal shape in the temporal wings. The glass–gas interface of the hollow fiber is depicted in light gray for comparison.

to the comparatively slow waveguide losses. This adiabatic scenario is contrasted by the use of hollow fibers for high-harmonic generation [48], where much shorter hollow fibers of smaller diameter are typically employed. Apart from the significantly increased modal dispersion, the already compressed input duration also requires consideration of shock terms [42], which we have left out in our analysis. In case of adiabatic reshaping, however, nonsolitonic contents are stripped off into linearly propagating higher-order modes, which travel at reduced group velocities. For example, for $a = 200$ μm and $\lambda = 1$ μm, the linear group velocity difference of the EH_{12} relative to the fundamental mode amounts to about 100 fs/m, i.e., the nonsolitonic contents will lead to the formation of a temporal continuum background after recompression. Ignoring reshaping effects due to group-velocity dispersion, one can now compute the structure of the emerging spatiotemporal light bullets; see Fig. 3. Here we have chosen the highest possible peak power in Fig. 2, i.e., $P = 1.4P_{cr}$, which leads to the formation of a donut spatial structure at the pulse center. At lower intensities, this structure goes over into the more common ellipsoidal shape of conventional light bullets. It needs to be emphasized that temporal broadening effects will accelerate the decrease of peak power. Yet, this effect of group-velocity dispersion can be easily compensated for by chirped mirrors. Uncompensated modal dispersion effects, however, cannot be fixed after nonlinear propagation in the fiber anymore. The severity of uncompensated intermodal dispersion becomes clear from reinspecting Fig. 1(d). An intermodal dispersion of 8 rad/cm between fundamental and EH_{14} modes results in a group delay of 140 fs in a 1 m long linear fiber, which needs to be compared with the typical sub-5 fs pulse duration of the compressed pulses observed after dispersion compensation.

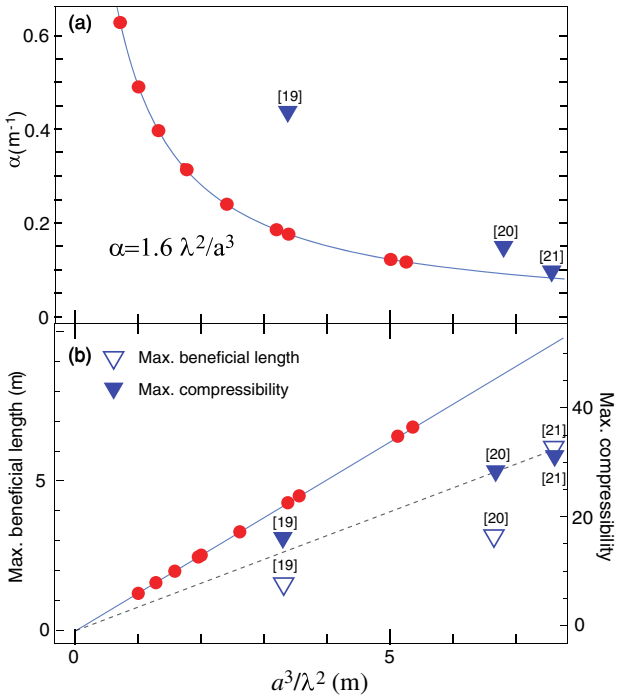

Fig. 4. Comparison of model results with measured data. (a) Total losses (linear and nonlinear) versus ratio of a^3 and λ^2 (curve and red dots). Early measurements with relatively short hollow fibers exhibited significantly higher losses, whereas more recent measurements showed excellent agreement as indicated by the respective references [19–21]. (b) Maximum beneficial length (solid curve and hollow triangles) and maximum compressibility (dashed line and solid triangles); cf. Eq. (13). This analysis confirms that superior compression can be reached with longer hollow fibers and larger core diameters.

5. HOLLOW-FIBER COMPRESSOR DESIGN RULES

Utilizing the spatial soliton solutions of Eq. (8), one can now derive a few design rules for hollow fiber compressors. As nonlinearly broadened spectra typically exhibit near-perfect spectral symmetry, one can employ the simple relation [41] derived for unchirped Gaussian input pulses,

$$\chi(z) = \frac{\Delta\nu_{\mathrm{rms}}}{\Delta\nu_0} = \sqrt{1 + \frac{4}{3\sqrt{3}}\varphi_{\mathrm{nl}}^2(z)}, \tag{13}$$

to estimate the compressibility of the input pulse. Here $\Delta\nu_0$ and $\Delta\nu_{\mathrm{rms}}$ are the input and output root mean square width of the pulse, respectively. In view of applications, increase of peak power is typically considered more important than ultimate shortness of the pulse. Let us therefore define the figure of merit,

$$M(a,\lambda) = \max[\chi(z)\exp(-2\alpha_{\mathrm{tot}}z)]|_z, \tag{14}$$

as the criterion for the maximum beneficial propagation length z_{max} inside the hollow fiber. This limit is reached when detrimental losses start to outweigh the higher compressibility that would result from additional spectral broadening. Consequently, neglecting any possible loss in the subsequent compression process (e.g., by chirped mirrors), peak powers will not further increase upon additional propagation. Pertinent computations are shown in Fig. 4, indicating the dependence of the total (linear and nonlinear) loss α_{tot} as a function of a^3/λ^2; see Fig. 4(a). Compared with experimental data [blue symbols in Fig. 4(a)], it appears striking that early work with relatively short fibers [19] reported losses that deviate from predictions of our model, whereas more recent reports with longer fibers [20,21] appear to completely agree with our model. Moreover, we also compare the maximum beneficial length and the observed spectral broadening between theory and previous experimental findings in Fig. 4(b). Here it is not overly surprising that our projections are too optimistic, with maximum compressibilities and beneficial fiber lengths that are about two-thirds of our predictions. Nevertheless, the relations derived from our spatial soliton model clearly explain the trends observed in previous experiments, confirming that long hollow fibers promise superior performance compared to the single-meter-long segments of early experimentation.

6. CONCLUSIONS

In conclusion, the field of multimode nonlinear optics bears a number of appealing applications, which are mostly ruled by an a^3/λ^2 relationship. In particular, in hollow fibers, where group-velocity dispersion plays an inferior role, spatial soliton

formation appears to take a previously unrecognized lead role at large diameters and lengths. Given that dispersive and absorptive lengths are orders of magnitude larger than the soliton length, adiabatic reshaping dominates the nonlinear dynamics of pulse propagation through the hollow fiber. As the critical power P_{cr} plays a decisive limiting role for the performance of a nonlinear multimode waveguide, further upscaling of compressible peak powers requires usage of lower pressures or gases with lower refractive index than the commonly used argon. As the currently demonstrated highest peak powers already used fibers with several-meter lengths, hosting even higher powers requires the use of significantly longer fibers of tens or even hundreds of meters' length to accumulate sufficient nonlinear phase for the broadening process. Such dimensions appear to be out of range for universities but could certainly be implemented in large-scale facilities, in particular linear accelerators. Using SCM fibers near their zero-dispersion wavelength instead, spectral broadening can be accomplished at much higher pulse energies than in single-mode fibers. In contrast to previous demonstrations of nonlinear multimode optics, our theoretical investigations suggest that the exact refractive index profile plays only a minor rule, enabling the use of simple step-index architectures rather than relying only on parabolic profiles.

Funding. Fundamental Research Funds for the Central Universities (00007475); CSC-DAAD (57460082).

Acknowledgment. G. S. gratefully acknowledges fruitful discussions with Pavel Sidorenko and Frank Wise (Cornell University), Boris Malomed (Tel Aviv University), as well as with Howard Milchberg (UMD).

Disclosures. The authors declare no conflicts of interest.

Data Availability. Data underlying the results presented in this paper are not publicly available at this time but may be obtained from the corresponding author upon reasonable request.

REFERENCES

1. R. Y. Chiao, E. Garmire, and C. H. Townes, "Self-trapping of optical beams," Phys. Rev. Lett. **14**, 1056 (1965).
2. V. E. Zakharov and A. B. Shabat, "Exact theory of two-dimensional self-focusing and one-dimensional self-modulation of waves in nonlinear media," Sov. Phys. JETP **34**, 62–69 (1972).
3. Y. Silberberg, "Collapse of optical pulses," Opt. Lett. **15**, 1282–1284 (1990).
4. K. D. Moll, A. L. Gaeta, and G. Fibich, "Self-similar optical wave collapse: observation of the Townes profile," Phys. Rev. Lett. **90**, 203902 (2003).
5. D. Majus, G. Tamošauskas, I. Gražulevičiūtė, N. Garejev, A. Lotti, A. Couairon, D. Faccio, and A. Dubietis, "Nature of spatiotemporal light bullets in bulk Kerr media," Phys. Rev. Lett. **112**, 193901 (2014).
6. V. I. Bespalov and V. I. Talanov, "Filamentary structure of light beams in nonlinear liquids," JETP Lett. **3**, 307–310 (1966).
7. E. S. Bliss, D. R. Speck, J. F. Holzrichter, J. H. Erkkila, and A. J. Glass, "Propagation of a high-intensity laser pulsewith small-scale intensity modulation," Appl. Phys. Lett. **25**, 448–450 (1974).
8. J. Marburger, "Self-focusing: theory," Prog. Quantum Electron. **4**, 35–110 (1975).
9. R. W. Boyd, *Nonlinear Optics*, 4th ed. (Academic, 2020).
10. E. Marcatili and R. Schmeltzer, "Hollow metallic and dielectric waveguides for long distance optical transmission and lasers," Bell Syst. Tech. J. **43**, 1783–1809 (1964).
11. M. Nisoli, S. De Silvestri, and O. Svelto, "Generation of high energy 10 fs pulses by a new pulse compression technique," Appl. Phys. Lett. **68**, 2793–2795 (1996).
12. M. Nisoli, S. De Silvestri, O. Svelto, R. Szipöcs, K. Ferenz, C. Spielmann, S. Sartania, and F. Krausz, "Compression of high-energy laser pulses below 5 fs," Opt. Lett. **22**, 522–524 (1997).
13. C. G. Durfee, A. R. Rundquist, S. Backus, C. Herne, M. M. Murnane, and H. C. Kapteyn, "Phase matching of high-order harmonics in hollow waveguides," Phys. Rev. Lett. **83**, 2187–2190 (1999).
14. S. Skupin, G. Stibenz, L. Bergé, F. Lederer, T. Sokollik, M. Schnürer, N. Zhavoronkov, and G. Steinmeyer, "Self-compression by femtosecond pulse filamentation: experiments versus numerical simulations," Phys. Rev. E **74**, 056604 (2006).
15. G. Jargot, N. Daher, L. Lavenu, X. Delen, M. H. N. Forget, and P. Georges, "Self-compression in a multipass cell," Opt. Lett. **43**, 5643–5646 (2018).
16. G. Sansone, E. Benedetti, F. Calegari, C. Vozzi, L. Avaldi, R. Flammini, L. Poletto, P. Villoresi, C. Altucci, R. Velotta, S. Stagira, S. De Silvestri, and M. Nisoli, "Isolated single-cycle attosecond pulses," Science **314**, 443–446 (2006).
17. X. Ma, J. Dostál, and T. Brixner, "Broadband 7-fs diffractive-optic-based 2D electronic spectroscopy using hollow-core fiber compression," Opt. Express **24**, 20781–20791 (2016).
18. T. Nagy, M. Forster, and P. Simon, "Flexible hollow fiber for pulse compressors," Appl. Opt. **47**, 3264–3268 (2008).
19. T. Nagy, V. Pervak, and P. Simon, "Optimal pulse compression in long hollow fibers," Opt. Lett. **36**, 4422–4424 (2011).
20. T. Nagy, S. Hädrich, P. Simon, A. Blumenstein, N. Walther, R. Klas, J. Buldt, H. Stark, S. Breitkopf, P. Jójárt, I. Seres, Z. Várallyay, T. Eidam, and J. Limpert, "Generation of three-cycle multi-millijoule laser pulses at 318 W average power," Optica **6**, 1423–1424 (2019).
21. T. Nagy, M. Kretschmar, M. J. J. Vrakking, and A. Rouzée, "Generation of above-terawatt 1.5-cycle visible pulses at 1 kHz by post-compression in a hollow fiber," Opt. Lett. **45**, 3313–3316 (2020).
22. G. Tempea and T. Brabec, "Theory of self-focusing in hollow waveguide," Opt. Lett. **23**, 762–764 (1998).
23. G. Fibich and A. Gaeta, "Critical power for self-focusing in bulk media and hollow waveguides," Opt. Lett. **25**, 335–337 (2000).
24. M. Nurhuda, A. Suda, K. Midorikawa, M. Hatayama, and K. Nagasaka, "Propagation dynamics of femtosecond laser pulses in a hollow fiber filled with argon: constant gas pressure versus differential gas pressure," J. Opt. Soc. Am. B **20**, 2002–2011 (2003).
25. J. Andreasen and M. Kolesik, "Midinfrared femtosecond laser pulse filamentation in hollow waveguides: a comparison of simulation methods," Phys. Rev. E **87**, 053303 (2013).
26. R. Safaei, G. Fan, O. Kwon, K. Légaré, P. Lassonde, B. E. Schmidt, H. Ibrahim, and F. Légaré, "High-energy multidimensional solitary states in hollow-core fibres," Nat. Photonics **14**, 733–739 (2020).
27. A. Crego, E. C. Jarque, and J. S. Roman, "Influence of the spatial confinement on the self-focusing of ultrashort pulses in hollow-core fibers," Sci. Rep. **9**, 9546 (2019).
28. B. A. López-Zubieta, E. C. Jarque, Í. J. Sola, and J. S. Roman, "Spatiotemporal-dressed optical solitons in hollow-core capillaries," OSA Contin. **1**, 930–938 (2018).
29. H. A. Haus, "Mode-locking of lasers," IEEE J. Sel. Top. Quantum Electron. **6**, 1173–1185 (2000).
30. E. Escoto, A. Demircan, and G. Steinmeyer, "Cage solitons," IEEE J. Quantum Electron. **57**, 1300106 (2021).
31. F. W. Wise, "Generation of light bullets," Physics **3**, 107 (2010).
32. W. H. Renninger and F. W. Wise, "Optical solitons in graded-index multimode fibres," Nat. Commun. **4**, 1719 (2013).
33. G. Lopez-Galmiche, Z. S. Eznaveh, M. A. Eftekhar, J. A. Lopez, L. G. Wright, F. Wise, D. Christodoulides, and R. A. Correa, "Visible supercontinuum generation in a graded index multimode fiber pumped at 1064 nm," Opt. Lett. **41**, 2553–2556 (2016).
34. L. G. Wright, P. Sidorenko, H. Pourbeyram, Z. M. Ziegler, A. Isichenko, B. A. Malomed, C. R. Menyuk, D. N. Christodoulides,

and F. W. Wise, "Mechanisms of spatiotemporal mode-locking," Nat. Phys. **16**, 565–570 (2020).
35. K. Krupa, A. Tonello, B. M. Shalaby, M. Fabert, A. Barthélémy, G. Millot, S. Wabnitz, and V. Couderc, "Spatial beam self-cleaning in multimode fibres," Nat. Photonics **11**, 237–241 (2017).
36. K. Krupa, A. Tonello, A. Barthélémy, T. Mansuryan, V. Couderc, G. Millot, P. Grelu, D. Modotto, S. A. Babin, and S. Wabnitz, "Multimode nonlinear fiber optics, a spatiotemporal avenue," APL Photon. **4**, 110901 (2019).
37. F. Goos and H. Hänchen, "Ein neuer und fundamentaler Versuch zur Totalreflexion," Ann. Phys. **436**, 333–346 (1947).
38. J. P. Crenn, "Optical study of the EH_{11} mode in a hollow circular oversized waveguide and Gaussian approximation of the far-field pattern," Appl. Opt. **23**, 3428–3433 (1984).
39. J. P. Crenn, "Optical propagation of the HE_{11} mode and Gaussian beams in hollow circular waveguides," Int. J. Infrared Millim. Waves **14**, 1947–1973 (1993).
40. A. W. Snyder and J. D. Love, *Optical Waveguide Theory* (Chapman and Hall, 1983).
41. G. P. Agrawal, *Nonlinear Fiber Optics*, 6th ed. (Academic, 2019).
42. F. Poletti and P. Horak, "Description of ultrashort pulse propagation in multimode optical fibers," J. Opt. Soc. Am. B **25**, 1645–1654 (2008).
43. R. N. Bracewell, *The Fourier Transform and Its Applications* (McGraw-Hill, 2000).
44. V. L. Vinetski, N. V. Kukhtarev, S. G. Odulov, and M. S. Soskin, "Dynamic self-diffraction of coherent light beams," Sov. Phys. Usp. **22**, 742–756 (1979).
45. K. W. DeLong, R. Trebino, and D. Kane, "Comparison of ultrashort-pulse frequency-resolved-optical-gating traces for three common beam geometries," J. Opt. Soc. Am. B **11**, 1595–1608 (1995).
46. R. T. Chapman, T. J. Butcher, P. Horak, F. Poletti, J. G. Frey, and W. S. Brocklesby, "Modal effects on pump-pulse propagation in an Ar-filled capillary," Opt. Express **18**, 13279–13284 (2010).
47. K. J. Blow, N. J. Doran, and S. J. D. Phoenix, "The soliton phase," Opt. Commun. **88**, 137–140 (1992).
48. A. Rundquist, C. G. Durfee, Z. H. Chang, C. Herne, S. Backus, M. M. Murnane, and H. C. Kapteyn, "Phase-matched generation of coherent soft X-rays," Science **280**, 1412–1415 (1998).